energies

MDPI

Article

An Innovative Metaheuristic Strategy for Solar Energy Management through a Neural Networks Framework

Hossein Moayedi [1,2,*] and Amir Mosavi [3,4,5,6,*]

[1] Institute of Research and Development, Duy Tan University, Da Nang 550000, Vietnam
[2] Faculty of Civil Engineering, Duy Tan University, Da Nang 550000, Vietnam
[3] Faculty of Civil Engineering, Technische Universität Dresden, 01069 Dresden, Germany
[4] School of Economics and Business, Norwegian University of Life Sciences, 1430 Ås, Norway
[5] John von Neumann Faculty of Informatics, Obuda University, 1034 Budapest, Hungary
[6] School of the Built Environment, Oxford Brookes University, Oxford OX3 0BP, UK
* Correspondence: hosseinmoayedi@duytan.edu.vn (H.M.); amir.mosavi@mailbox.tu-dresden.de (A.M.)

Abstract: Proper management of solar energy as an effective renewable source is of high importance toward sustainable energy harvesting. This paper offers a novel sophisticated method for predicting solar irradiance (SIr) from environmental conditions. To this end, an efficient metaheuristic technique, namely electromagnetic field optimization (EFO), is employed for optimizing a neural network. This algorithm quickly mines a publicly available dataset for nonlinearly tuning the network parameters. To suggest an optimal configuration, five influential parameters of the EFO are optimized by an extensive trial and error practice. Analyzing the results showed that the proposed model can learn the SIr pattern and predict it for unseen conditions with high accuracy. Furthermore, it provided about 10% and 16% higher accuracy compared to two benchmark optimizers, namely shuffled complex evolution and shuffled frog leaping algorithm. Hence, the EFO-supervised neural network can be a promising tool for the early prediction of SIr in practice. The findings of this research may shed light on the use of advanced intelligent models for efficient energy development.

Keywords: solar irradiance; solar energy; solar power; electrical power modeling; metaheuristic; machine learning; artificial neural networks; artificial intelligence; big data; deep learning; photovoltaic

Citation: Moayedi, H.; Mosavi, A. An Innovative Metaheuristic Strategy for Solar Energy Management through a Neural Networks Framework. *Energies* **2021**, *14*, 1196. https://doi.org/10.3390/en14041196

Academic Editor: Maurizio De Lucia

Received: 3 January 2021
Accepted: 19 February 2021
Published: 23 February 2021

1. Introduction

Today, solar energy (SE) is considered a promising renewable source because of its advantages, such as inexhaustible supply, environmental friendliness, universality, and high capacity [1,2]. Indeed, the term artificial intelligence is known as intelligence demonstrated by machines (i.e., unlike natural intelligence, which involves emotionality and consciousness shown by animals and humans). In this sense, intelligence approaches have provided a high degree of suitability for undertaking complicated and nonlinear simulations [3–5]. Most recently, a number of innovative artificial-intelligence-based examples have been studied, such as in the subjects of environmental concerns [6–14], sustainability [15], soil precipitation and pan evaporation prediction [16–21], energy systems optimization [22–34], energy efficiency [35], natural gas consumption [36–39], water and groundwater supply chains [9,40–49], image classification and processing, computer vision, and target tracking [50–58], structural damage detection [59], building and structural design analysis [54,60–64], quantifying climatic contributions [65], measurement techniques [50,66–68], the behavior of structural materials [65,69–71], and signal processing and feature analysis [72–78]. Many decision-making issues have been proposed for engineering modelings [54,79,80]. As a mimic of human brain operations, the artificial neural network (ANN) is founded on a set of algorithms aiming to recognize underlying correspondence among a group of input–output data [81–85]. In another sense, the ANN represents a sophisticated nonlinear approach that has been proposed as a popular tool for

different modeling tasks [86]. Among various notions of the ANNs, multi-layer perceptron (MLP) [87,88] is an important one composed of (at least) three layers. Each layer contains one or more neurons that handle the computation tasks [89–94]. As some medical applications of machine learning, scholars like Xia, et al. [95], Hu, et al. [96], Wang, et al. [97], and Chen, et al. [98] have achieved satisfying solutions.

Having a reliable forecast of solar irradiance (SIr) is of great importance, due to its effect on the design of photovoltaic systems and measuring solar energy production [99,100]. Figure 1 shows solar radiation on a photovoltaic module installed on the Earth. Up to now, scholars have suggested various methods (e.g., empirical [101] and remote sensing [102] approaches) for analyzing the SE parameter. However, recent advances in soft computing have led to the utilization of diverse machine learning tools for this purpose. These modes have gained a lot of attention for renewable energy analysis like feature selection [103].

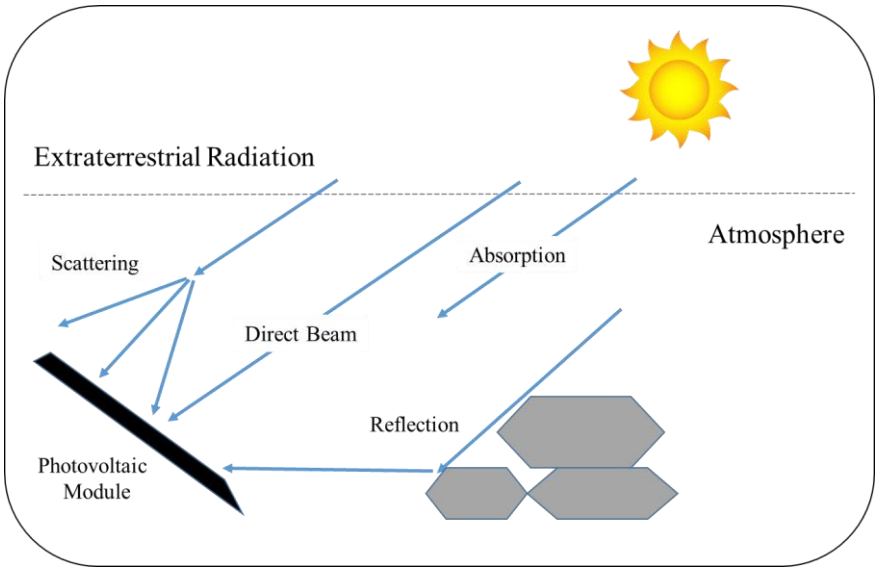

Figure 1. A schematic view of solar radiation and solar energy (SE) production.

Artificial neural network (ANN), for example, is a flexible type of machine learning that has been broadly used for prediction tasks. Barrera, et al. [104] proposed an ANN model developed with open data sources for analyzing SE and also the effect of environmental factors on this parameter. The used model was found to be more accurate than previous methods (with a mean square error (MSE) of 0.040 vs. 0.055). Yaïci, et al. [105] demonstrated the effectiveness of ANN for simulating the SE systems. They also investigated the effect of the problem dimension (i.e., the number of inputs) on the accuracy, and after testing the model using real-world (Ottawa, Canada) data, they professed that the accuracy falls gradually with reducing the dimension. Yadav, et al. [106] conducted a comparison among different ANN models, namely radial basis function neural network (RBFNN), fitting tool (nftool), and generalized regression neural network (GRNN), for analyzing the potential of SE resources in India. They reported the superiority of the nftool, as it could nicely predict the desired parameter for many locations.

Meenal and Selvakumar [107] studied and demonstrated the accuracy of a popular machine learning system called support vector machine (SVM) for solar radiation modeling. This method, when implemented with an optimal dataset, outperformed the ANN and empirical approaches for this purpose. Mohammadi, et al. [108] performed a feature analysis using another well-known processor, namely the adaptive neuro-fuzzy inference system (ANFIS) for global solar radiation modeling. Quej, et al. [109] compared the potential of ANN, SVM, and ANFIS for simulating daily solar radiation. Concerning the respective average correlations of 0.652, 0.689, and 0.645 obtained for the best models, the SVM emerged as the most reliable predictor.

Metaheuristic algorithms have paved the way for more powerful forecasting models that are using the skeleton of conventional tools like ANN and ANFIS. These algorithms have been popularly used for renewable energy analysis [110,111] like wind energy [112,113], solar power energy [114], and, more particularly, the SE-related simulations [115,116]. In such methodologies (i.e., metaheuristic-based hybrids) optimal parameters are provided for the basic predictive method to avoid issues like local minima [117]. Many scholars investigated proposing hybrid metaheuristic algorithms that intend to improve the level of algorithm performance. Some of these hybrid algorithms are the whale optimization algorithm [118,119], grey wolf optimization [120,121], the many-objective optimization model [122–125], moth-flame optimization [126–128], Monarch Butterfly optimization [129], harris hawks optimization [130,131], bacterial foraging optimization [132], global numerical optimization [133], the grasshopper optimization algorithm [134], fruit fly optimization [135], data-driven robust optimization [136], topology optimization [137], multiobjective 3-d topology optimization [138], and the fuzzy optimization strategy [139].

Abedinia, et al. [140] designed a forecast engine based on a metaheuristic optimizer called shark smell optimization combined with ANN for approximating solar power. Due to the better performance of this model in comparison with conventional predictors like conventional ANN, RBFNN, GRNN, and their wavelet versions (normalized root mean square errors (RMSEs) around 11 vs. those above 14), they introduced it as a capable engine. Galván, et al. [141] benefitted from a multi-objective particle swarm optimization (PSO) technique for optimizing the intervals of the SE modeling. They built a nonlinear method using ANN, and their findings revealed the high applicability of the PSO optimizer for the mentioned objective. Zhao, et al. [142] employed two metaheuristic techniques, namely shuffled complex evolution (SCE) and Teaching–Learning-Based Optimization (TLBO), to predict the compressive strength of concrete. Likewise, Halabi, et al. [143] could effectively use this algorithm coupled with an ANFIS system for monthly solar radiation approximation. Vaisakh and Jayabarathi [144] suggested a hybrid of two methods, namely the deer hunting optimization algorithm and grey wolf optimization, for tuning the structure of various ANNs applied to SIr forecast. Their results showed a promising improvement attained by the proposed optimizer. Louzazni, et al. [145] showed the competency of the firefly algorithm for analyzing the parameters of the photovoltaic system under different conditions. Compared to previously used metaheuristic techniques, the firefly algorithm achieved reliable and valid results in tuning the photovoltaic parameters. The efficiency of the PSO and genetic algorithm (GA) for a similar objective was demonstrated by Bechouat, et al. [146]. Wind-driven optimization was successfully used by Abdalla, et al. [147] to deal with the optimal power tracking of photovoltaic systems. This algorithm performed more efficiently than several optimization techniques, such as PSO, the bat algorithm, and cuckoo search.

According to the explained literature, metaheuristic algorithms can yield promising solutions to complex issues like SIr prediction. However, a gap in knowledge has emerged as earlier studies have mostly used well-established strategies like PSO [148], GA [149], and the imperialist competitive algorithm [150]. Furthermore, these techniques take a noticeable time to reach stable optimization. This study, therefore, focuses on a novel metaheuristic strategy, namely electromagnetic field optimization (EFO), for the optimal prediction of the SIr. A significant advantage of this algorithm is its fast convergence relative to other existing techniques. The EFO supervises a nonlinear problem through an ANN framework. Moreover, two other quick algorithms, shuffled complex evolution (SCE) and the shuffled frog leaping algorithm (SFLA), are considered benchmark methods to comparatively validate the efficiency of the EFO.

2. Materials and Methods

2.1. Data Provision

For predicting the SIr, a publicly available dataset (provided by NASA and available at https://www.kaggle.com/dronio/SolarEnergy, accessed on 26 October 2020) is used in

this work. Before this study, these data have been used for validating the performance of different developed models [151,152]. The SIr plays the role of the target parameter to be predicted with the inputs of temperature (T), barometric pressure (BP), humidity (H), wind direction (WD), and wind speed (WS).

The used dataset contains 32,686 rows of meteorological records obtained from the Hawaii space exploration analog and simulation (HI-SEAS) weather station. At approximately 5 minute intervals, the records belong to the time between 23:55:26 29 September 2016 and 00:00:02 1 December 2016. Figure 2 shows the variation of the SIr over one day (29 September 2016 taken as an instance). As expected, peak values are observed at midday. Moreover, Figure 3 depicts the relationship between the SIr and each input factor in the form of scatter charts for the whole dataset.

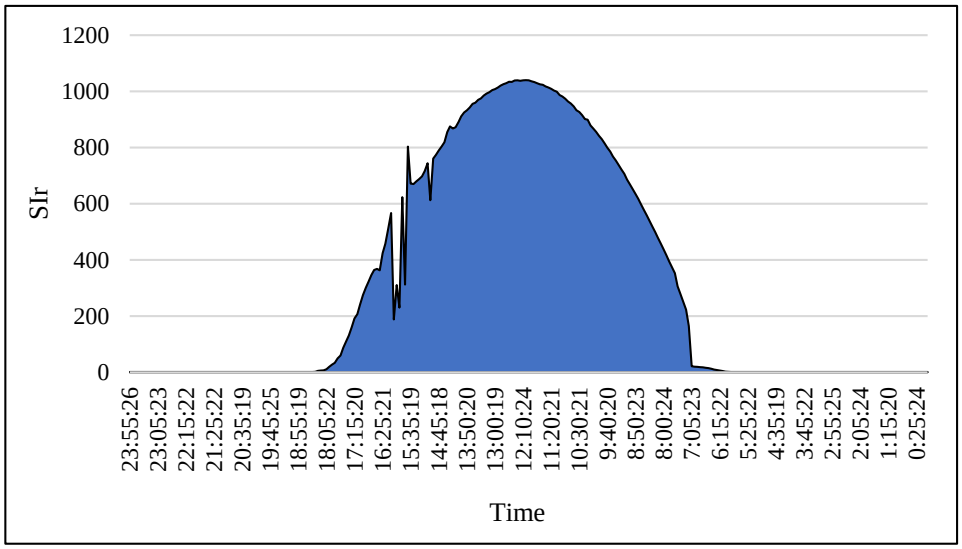

Figure 2. The variation of the solar irradiance (SIr) over 29 September 2016.

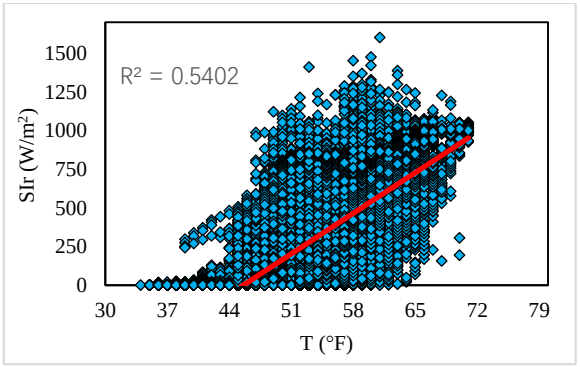

(**a**)

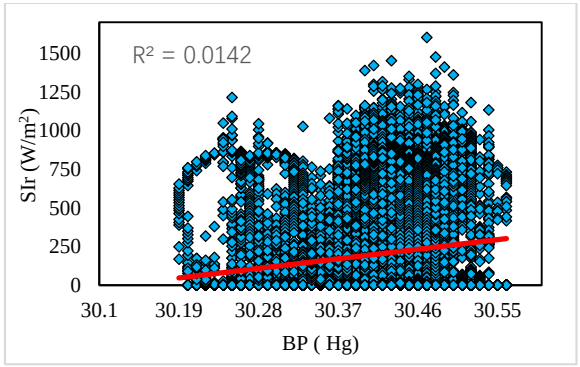

(**b**)

Figure 3. *Cont.*

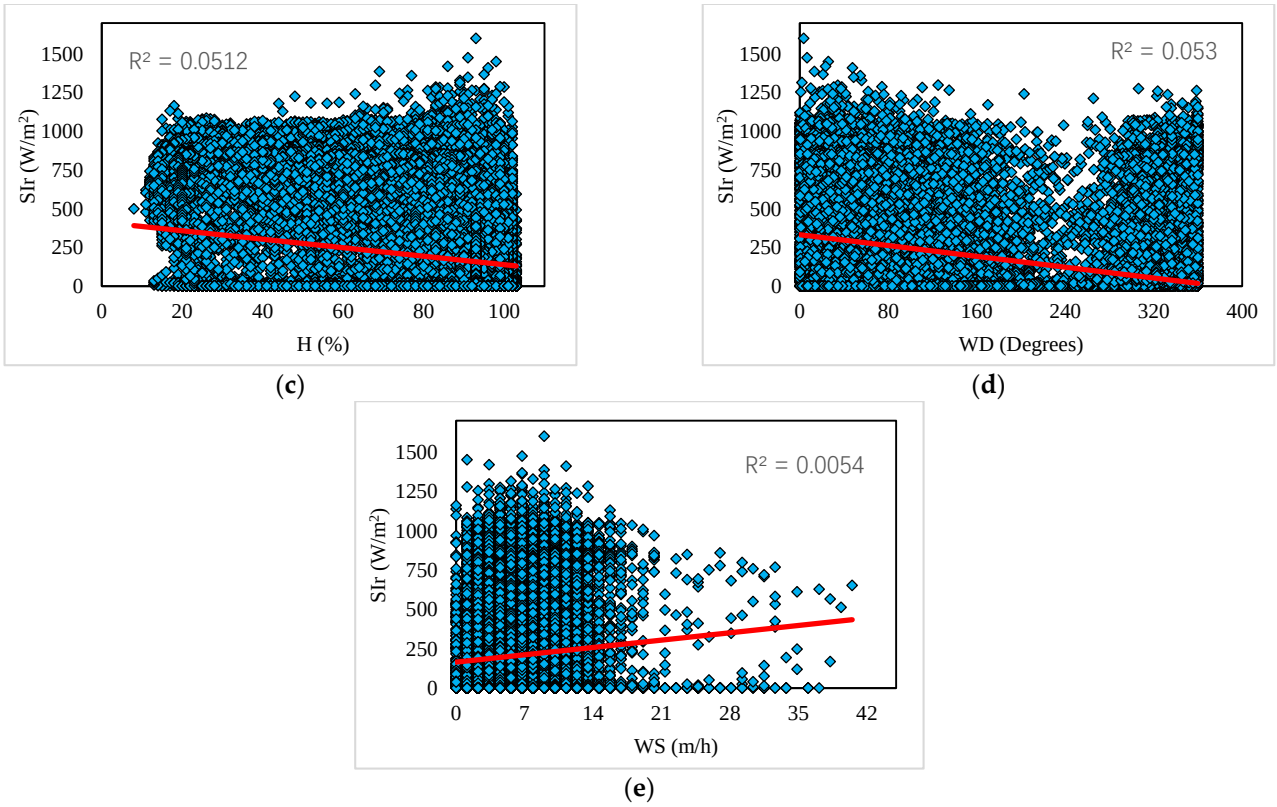

Figure 3. Scattering plots of the SIr versus input parameters (**a**) T, (**b**) BP, (**c**) H, (**d**) WD, and (**e**) WS.

Considering the R^2 values calculated in Figure 3 (0.5402, 0.0142, 0.0512, 0.053, and 0.0054 for the T, BP, H, WD and WS, respectively), it can be said that the most meaningful relationship (among these five inputs) is obtained for the T. In a general view, the values of SIr tend to increase with the increase in this factor. A detailed statistical description of the used dataset is presented in Table 1. As is seen, the SIr values range over [1.1, 1601.3] W/m2, while this extent is [34.0, 71.0] °F, [30.2, 30.6] Hg, [8.0, 103.0] %, [0.1, 360.0] degrees, and [0.0, 40.5] m/h for the T, BP, H, WD, and WS, respectively.

Table 1. Descriptive statistics of the SIr and input parameters.

Factor	Unit	Descriptive Indicator					
		Mean	Std. Error	Std. Deviation	Sample Variance	Minimum	Maximum
T	°F	51.1	0.0	6.2	38.5	34.0	71.0
BP	Hg	30.4	0.0	0.1	0.0	30.2	30.6
H	%	75.0	0.1	26.0	675.5	8.0	103.0
WD	Degree	143.5	0.5	83.2	6916.8	0.1	360.0
WS	m/h	6.2	0.0	3.5	12.2	0.0	40.5
SIr	W/m2	207.1	1.7	315.9	99,803.2	1.1	1601.3

In artificial intelligence implementation, it is well-established that machines use some (the majority) of the instances for learning the existing input-target pattern. They then apply this pattern to the remaining instances for evaluating the prediction ability. For this study, the dataset (i.e., 32,686 instances) was randomly divided into two groups with 26,149 and 6537 instances (80% and 20% of the whole) to generate the training and testing dataset, respectively.

Since the data are randomly selected, there are samples from all over the dataset in both the training and tested boxes. However, the scattering and broadness of data (Figure 3) indicate that the predictive models deal with a wide variety of data (e.g., an SIr value with

similar temperature and barometric pressure) that make the problem intrinsic. Thus, it can be another factor for evaluating the generalizability of the used models.

2.2. Methodology

2.2.1. The EFO

Abedinpourshotorban, et al. [153] developed a physics-based optimization strategy and named it electromagnetic field optimization. Many scholars have benefited from this method for a wide range of problems [154,155]. It is a population-based technique in which each individual is represented by an electromagnetic particle (EMP). The EMPs are distinguished by different polarities. The attraction–repulsion rule is used to improve the solution by changing the position of the EMPs.

The steps of the EFO can be explained as follows:

Step 1: A set of EMPs are randomly generated and the fitness of each one is calculated. The particles are then sorted based on these fitnesses. Each particle is made of N_var electromagnets (tantamount to the number of problem variables).

Step 2: This is dedicated to dividing the EMP population into three field groups with negative, positive, and neutral polarities. The positive field group comprises the best-fitted individuals tunable by a so-called "P_field" parameter, the negative field group comprises the worst-fitted individuals tunable by a so-called "N_field" parameter, and the rest lie in the third group.

Step 3: Each repetition of the algorithm generates a new EMP. Once this EMP is better fitted than the weakest one, it is considered as a part of the population and confiscates the position of the weakest EMP. Figure 4 shows the generation process and determination on the polarity of the new member.

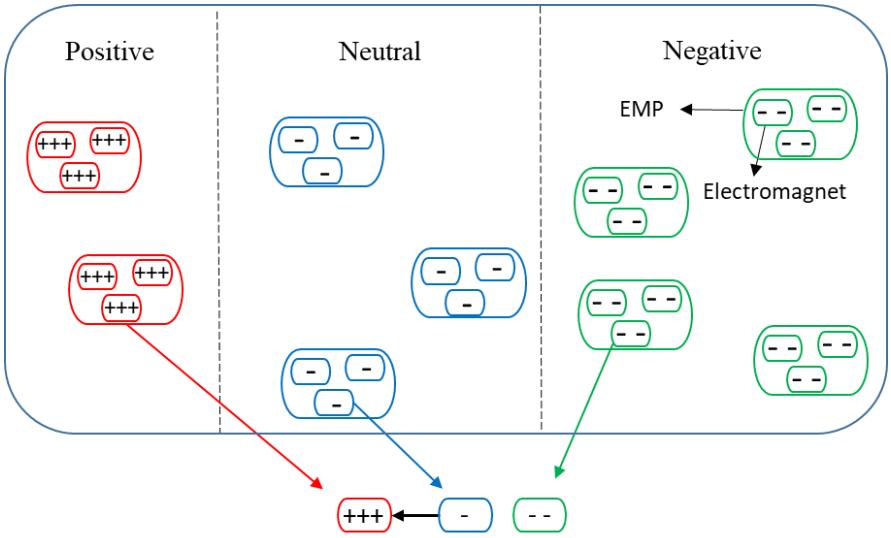

Figure 4. The creation of a new electromagnetic particle (EMP).

In this process, for j = 1 → N_var, an electromagnet belonging to the neutral field group is chosen. Next, a random value is considered and compared to a parameter called Ps_rate, which indicates the probability of choosing electromagnets of the created EMP from the positive field. Equation (1) is used for the situation random value <Ps_rate; otherwise, Equation (2) expresses the generation process.

$$EMP_j^{new} = EMP_j^{PF_j}, \quad (1)$$

$$EMP_j^{new} = EMP_j + (GR * rand) \times \left(EMP_j^{PF_j} - EMP_j \right) + (rand) \times \left(EMP_j^{NF_j} - EMP_j \right), \quad (2)$$

where *PF* and *NF* symbolize positive and negative fields, *GR* gives the golden ratio, and *rand* is the random value inside [0, 1].

Step 4: A randomization operator is responsible for diversifying the new EMPs. Another random value is generated and compared to a parameter called R_rate, which indicates the probability of replacing one electromagnet of the created EMP with a random electromagnet. If random value <R_rate, a new electromagnet replaces one electromagnet of the created EMP [155].

2.2.2. The Benchmarks

The SCE and SFLA are efficient metaheuristic techniques that are used as comparative methods in this work. While both algorithms are based on shuffle action, the SCE is an older optimizer. Duan, et al. [156] and Eusuff and Lansey [157] presented the SCE and SFLA in 1993 and 2003, respectively. Although this study is one of the first usages of the EFO for supervising an ANN, scholars like Zheng, et al. [42] and Ma, et al. [158] have reported successful performance of the SCE and EFO for this purpose.

The SCE implements a combination of the Nelder–Mead simplex technique, genetic algorithm, complex shuffling, and controlled random search for doing the optimization. After creating the population, the individuals are grouped in some containers called complexes. The algorithm uses competitive complex evolution for evolving these complexes. It then synthesizes evolved units to create a larger community. This step results in more interactive agents for better sharing of the obtained knowledge [159]. The pivotal idea of the SFLA is the relationship between frogs settled in some containers called memeplexes. It is known as a quick and efficient search scheme that synthesizes PSO with the memetic algorithm. The fitness of the frogs is a measure for classifying them as the memeplexes. The SFLA pursues updating the position of the frogs in these units, and also importing new ones instead of the worst individuals [160]. The benchmark algorithms are mathematically detailed in earlier studies like [161,162] (for the SCE) and [163,164] (for the SFLA).

Similar to the EFO, two separate ANNs are supervised by the benchmark algorithms to explore and predict the SIr. The performance of these three methods is compared in the following sections to return an optimal metaheuristic-based methodology for this purpose.

3. Results and Discussion

3.1. Accuracy Assessment Measures

The accuracy of SIr prediction is reported by well-known indices as follows. Given $Error_i = SIr_{i_{recorded}} - SIr_{i_{predicted}}$, the error of prediction for a total of N instances is calculated by the RMSE and mean absolute error (MAE) indices. According to Equations (3) and (4), the RMSE gives a rooted value of the averaged squared errors, while the MAE releases an average of the absolute error values.

$$\text{RMSE} = \sqrt{\frac{1}{N}\sum_{i=1}^{N}[Error_i]^2}, \tag{3}$$

$$\text{MAE} = \frac{1}{N}\sum_{i=1}^{N}|Error_i|, \tag{4}$$

A correlation index called Pearson correlation coefficient (R) is also defined to show the consistency between the recorded SIrs and the products of each network. Equation (5) formulates the R:

$$\text{R} = \frac{\sum_{i=1}^{N}(SIr_{i_{predicted}} - \overline{SIr}_{predicted})(SIr_{i_{recorded}} - \overline{SIr}_{recorded})}{\sqrt{\sum_{i=1}^{N}(SIr_{i_{predicted}} - \overline{SIr}_{predicted})^2}\sqrt{\sum_{i=1}^{N}(SIr_{i_{recorded}} - \overline{SIr}_{recorded})^2}} \tag{5}$$

where $\overline{SIr}$ symbolizes the average of the *SIr* values.

3.2. Optimization and Training

A 5 × 45 × 1 MLP neural network (indicating 5 nodes in the input layer, 45 nodes in the middle layer, and 1 node in the output layer) is used to connect the SIr to its input factors. Due to a large number of data instances, this network is a complex system that is supposed to be supervised by the EFO algorithm. The main role of the EFO is to adjust the MLP internal parameters so that the SIr pattern is optimally established.

After creating the EFO-MLP hybrid, it is trained by mining the training group. Since metaheuristic algorithms are population-based iterative techniques, optimum values should be considered for these two parameters, i.e., population size (N_{Pop}) and the number of iterations (NIt). Although many optimization algorithms reach a stable situation by around 1000 iterations, the EFO needs more effort. Based on experience and also evaluating the behavior of the model, the EFO-MLP was implemented by a total of 50,000 iterations. The appropriate values for N_{Pop}, as well as four other parameters, were determined one by one by testing different values. The convergence curves of the tested EFO-MLPs are shown in Figure 5. First, the models with different N_{Pop}s (25, 26, 27, 28, 30, 35, and 40) were tested (when R_rate = 0.01, Ps_rate = 0.01, P_field = 0.02, and N_field = 0.4). Figure 5a shows that the N_{Pop} = 26 gives the lowest error. Thus, the subsequent models were tested with this N_{Pop}. Five R_rates of 0.01, 0.015, 0.02, 0.03, and 0.04 were similarly assessed. According to Figure 5b, R_rate = 0.01 is the most suitable one. Next, investigating the effect of Ps_rate in Figure 5c revealed that the lowest error is obtained for Ps_rate = 0.03. As is exhibited in Figure 5d, P_field experienced the values of 0.02, 0.03, 0.04, 0.05, and 0.06, and P_field = 0.02 remained as the best value. Lastly, the values considered for N_field, 0.1, 0.2, 0.3, 0.4, and 0.5, are depicted in Figure 5e, which demonstrates the lowest error for N_field = 0.4.

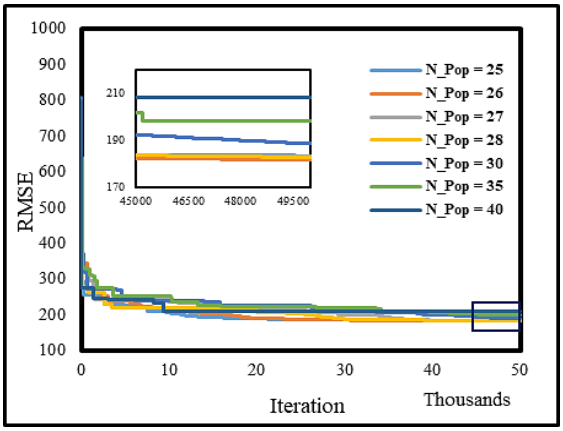

(**a**)

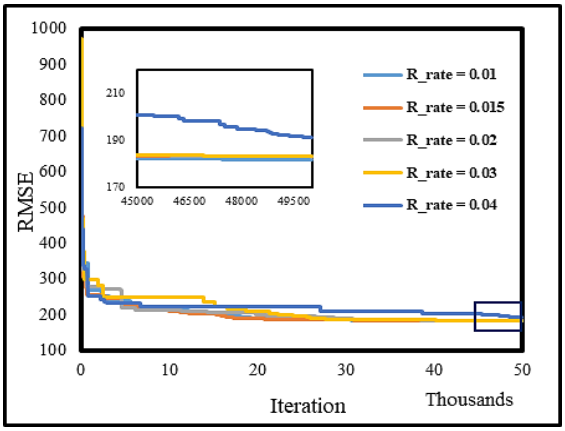

(**b**)

Figure 5. *Cont.*

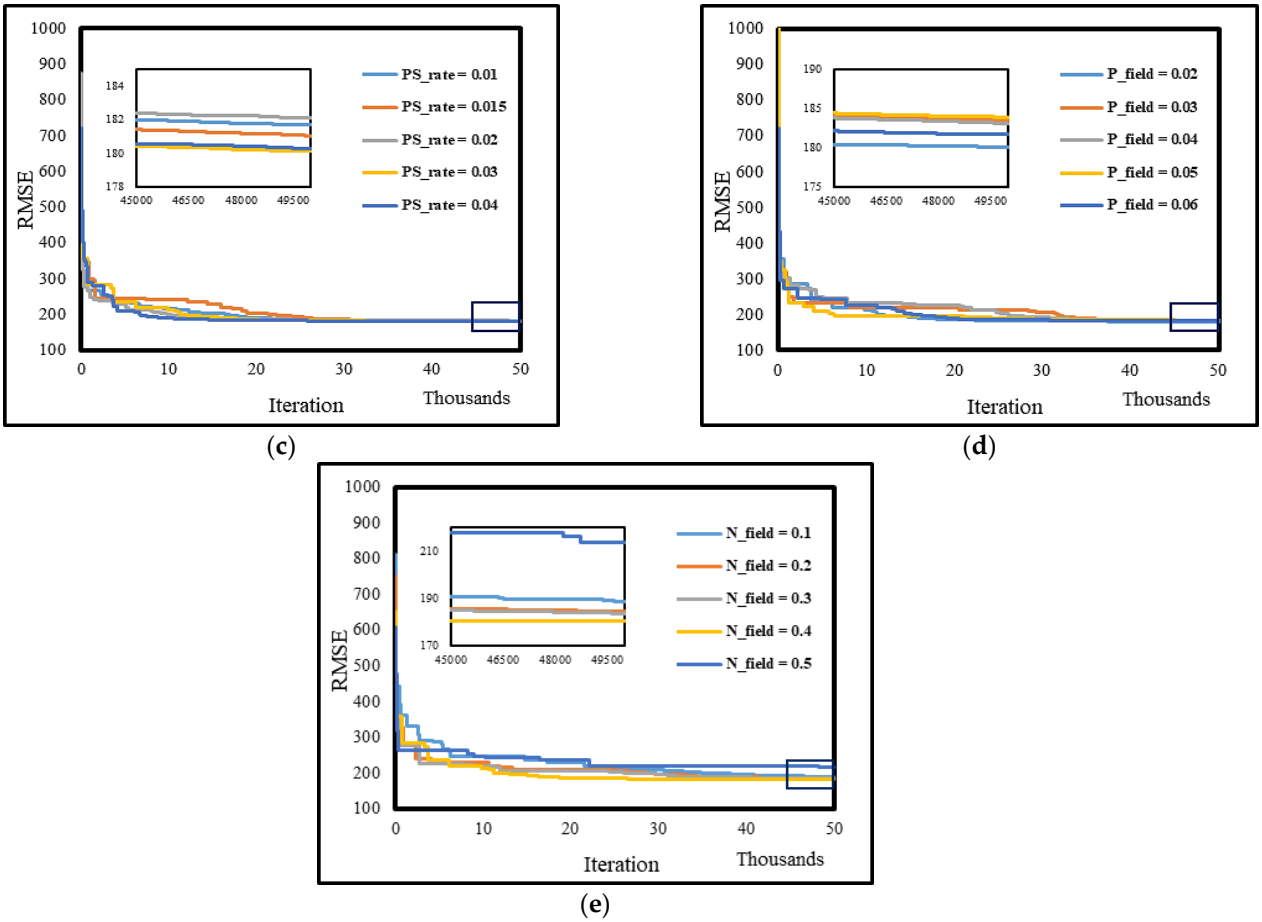

Figure 5. Optimizing the effect of electromagnetic field optimization (EFO) parameters including (**a**) N_{Pop}, (**b**) R_rate, (**c**) Ps_rate, (**d**) P_field, and (**e**) N_field.

A similar strategy was executed for the benchmark models (i.e., SCE-MLP and SFLA-MLP). Table 2 denotes the values assigned to the used algorithms. As is seen, the SCE and SFLA were implemented with 1000 iterations.

Table 2. Implementation parameters of the used algorithms.

EFO	SCE	SFLA
NPop = 26 R_rate = 0.01 Ps_rate = 0.01 P_field = 0.02 N_field = 0.4 NIt = 50,000	NPop = 10 No. of offsprings = 3 No. of complexes = 3 NIt = 1000	NPop = 25 Step size = 1 No. of offsprings = 3 No. of memeplexes = 5 NIt = 1000

Assessing the RMSEs obtained for the EFO-MLP, SCE-MLP, and SFLA-MLP, which are 180.1228, 197.4813, and 208.1472, respectively, shows that the used hybrids could learn the SIr pattern with good accuracy. The corresponding MAEs are 117.8681, 138.5814, and 156.2768, which, regarding the range of the observed SIrs (Table 1), indicate an acceptable level of error. Moreover, the correlation values of 0.82275, 0.78208, and 0.75431 demonstrate a high agreement between the training products and expected SIrs.

3.3. Testing Results

As explained in Section 2, the second part of the dataset plays the role of unseen environmental conditions. The models use this data to evaluate their testing ability. In this

regard, the SIr is forecasted for the testing instances and these values are compared with the expected values. Since the model does not perform any analysis on these instances, it has to use the previously captured knowledge. Accordingly, the goodness of the results reflects the prediction capability of the intended model.

Considering the $Error_i$ formula (Section 3.1), Figure 6 details the magnitude and statistics of error values calculated for the testing instances. In this phase, the RMSEs of 177.9764, 195.0984, and 205.6091 indicated a reliable prediction by all three models. Moreover, the goodness of the testing results can be supported by the MAEs of 115.2678, 136.2261, and 154.1603, as well as the R values of 0.82132, 0.78046, and 0.75212.

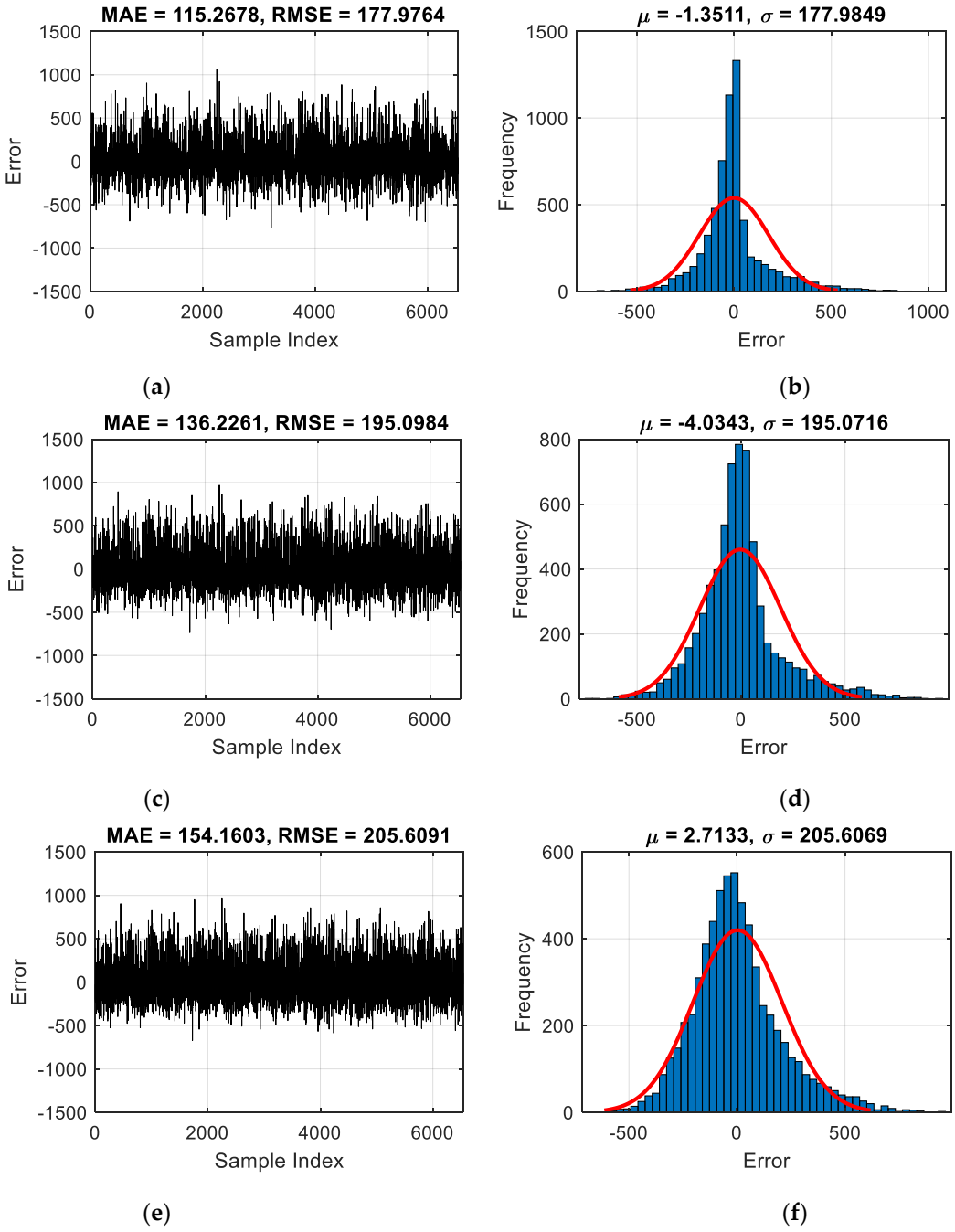

Figure 6. The error analysis in terms of (**a**,**c**,**e**) magnitude and (**b**,**d**,**f**) frequency for the EFO-multi-layer perceptron (MLP), shuffled complex evolution (SCE)-MLP, and shuffled frog leaping algorithm (SFLA)-MLP, respectively.

Moreover, from a graphical point of view, the histogram charts in Figure 6 show that the small errors outnumber large values. This can be derived from the sharp shape of the diagram around zero and the vicinity. Regarding the overall trend of these charts, the magnitude of the error increases as the frequency falls.

3.4. EFO vs. SCE and SFLA

It was stated that this research pursues a novel time-efficient methodology for analyzing the SIr. The EFO was presented as the pivotal method, while the SCE and SFLA acted as benchmark algorithms. Earlier sections showed the competency of all three supervised models. Hence, this section validates the performance of the EFO versus the SCE and SFLA.

For both training and testing groups, the error indicators showed a lower error of prediction, and, at the same time, the R index manifested a higher correlation for the EFO-trained model. Table 3 gives the accuracy improvements when the SCE and SFLA are replaced with the EFO. As is seen, in the case of EFO vs. SCE, the RMSE and MAE fall by nearly 10% and 18% in both phases, respectively. Additionally, a 4% enhancement resulted for the R index. As for EFO vs. SFLA, the changes are more tangible. The RMSE and MAE of both phases degrade by around 16% and 33%, respectively. The R index indicated a 7% better correlation, too.

Table 3. Improvements achieved by the EFO algorithm vs. the benchmarks.

Comparative Hybrid	Improvements					
	Training Phase			Testing Phase		
	RMSE (%)	MAE (%)	R^2	RMSE (%)	MAE (%)	R^2
Vs. SCE	9.64	17.57	0.04	9.62	18.18	0.04
Vs. SFLA	15.56	32.59	0.07	15.53	33.74	0.07

4. Conclusions

This research was dedicated to finding a fast yet reliable solution for predicting solar irradiance. Since this parameter is affected by different factors, the problem is a nonlinear complex one. Therefore, a potent metaheuristic strategy called electromagnetic field optimization was considered for dealing with it. A neural network organized the general equations while the EFO tuned its parameters optimally. Moreover, this algorithm was compared with two shuffle-based metaheuristic techniques: the shuffled frog leaping algorithm and shuffled complex evolution. While an adequate level of accuracy was observed for all three hybrids, the EFO-MLP was significantly superior. For example, its error was around 10% and 16% below that of the SCE-MLP and SFLA-MLP, respectively. Referring to the R-value of 0.82132 for testing data, the proposed model can reliably predict the SIr for given environmental conditions. In comparison with other hybrid techniques such as SCE and SFLA, the EFO showed better performance. The employed accuracy indices for the applied benchmark technique (i.e., RMSE, MAE, and R2) were 9.64, 17.57, and 0.04 (vs. SCE) and 15.56, 32.59, and 0.07 (vs. SCE) for the used training dataset, and were 9.62, 18.18, and 0.04 (vs. SCE) and 15.53, 33.74, and 0.07 (vs. SCE) for the testing dataset. Having both in mind, the EFO algorithm could provide a more accurate predictive network in predicting the outputs. Apart from the high implementation speed, another advantage of the used EFO-MLP model lies in implementing optimized parameters (i.e., Npop, R_rate, Ps_rate, P_field, and N_field). Therefore, the findings of this study can be used for sustainable energy management. However, there may still be ideas for future works (e.g., using feature selection and filtrated data) for a more efficient methodology. Applying the developed method to other real-world sites can better reveal the advantages and drawbacks. Additionally, comparing the EFO with other capable optimizers or employing hybrids, ensemble and deep machine learning methods would be of high interest.

Author Contributions: Conceptualization, H.M.; methodology, software, validation, writing—original draft preparation, A.M.; writing—review and editing, visualization, supervision. All authors have read and agreed to the published version of the manuscript.

Funding: This research received no funding.

Institutional Review Board Statement: Not applicable.

Informed Consent Statement: Not applicable.

Data Availability Statement: Not applicable.

Conflicts of Interest: The authors declare no conflict of interest.

References

1. Gong, J.; Li, C.; Wasielewski, M.R. Advances in solar energy conversion. *Chem. Society Rev.* **2019**, *48*, 1862–1864. [CrossRef]
2. Mofijur, M.; Mahlia, T.M.I.; Silitonga, A.S.; Ong, H.C.; Silakhori, M.; Hasan, M.H.; Putra, N.; Rahman, S. Phase change materials (PCM) for solar energy usages and storage: An overview. *Energies* **2019**, *12*, 3167. [CrossRef]
3. Liu, Z.; Shao, J.; Xu, W.; Chen, H.; Zhang, Y. An extreme learning machine approach for slope stability evaluation and prediction. *Nat. Hazards* **2014**, *73*, 787–804. [CrossRef]
4. Piotrowski, A.P.; Osuch, M.; Napiorkowski, M.J.; Rowinski, P.M.; Napiorkowski, J.J. Comparing large number of metaheuristics for artificial neural networks training to predict water temperature in a natural river. *Comput. Geosci.* **2014**, *64*, 136–151. [CrossRef]
5. Liu, J.; Wu, C.; Wu, G.; Wang, X. A novel differential search algorithm and applications for structure design. *Appl. Math. Comput.* **2015**, *268*, 246–269. [CrossRef]
6. Feng, S.; Lu, H.; Tian, P.; Xue, Y.; Lu, J.; Tang, M.; Feng, W. Analysis of microplastics in a remote region of the Tibetan Plateau: Implications for natural environmental response to human activities. *Sci. Total Environ.* **2020**, *739*, 140087. [CrossRef]
7. Fu, X.; Fortino, G.; Pace, P.; Aloi, G.; Li, W. Environment-fusion multipath routing protocol for wireless sensor networks. *Inf. Fusion* **2020**, *53*, 4–19. [CrossRef]
8. Han, X.; Zhang, D.; Yan, J.; Zhao, S.; Liu, J. Process development of flue gas desulphurization wastewater treatment in coal-fired power plants towards zero liquid discharge: Energetic, economic and environmental analyses. *J. Clean. Prod.* **2020**, *261*, 121144. [CrossRef]
9. He, L.; Chen, Y.; Zhao, H.; Tian, P.; Xue, Y.; Chen, L. Game-based analysis of energy-water nexus for identifying environmental impacts during Shale gas operations under stochastic input. *Sci. Total Environ.* **2018**, *627*, 1585–1601. [CrossRef]
10. He, L.; Shen, J.; Zhang, Y. Ecological vulnerability assessment for ecological conservation and environmental management. *J. Environ. Manag.* **2018**, *206*, 1115–1125. [CrossRef]
11. Liu, J.; Liu, Y.; Wang, X. An environmental assessment model of construction and demolition waste based on system dynamics: A case study in Guangzhou. *Environ. Sci. Pollut. Res.* **2020**, *27*, 37237–37259. [CrossRef]
12. Liu, Y.; Yang, C.; Sun, Q. Thresholds Based Image Extraction Schemes in Big Data Environment in Intelligent Traffic Management. *IEEE Trans. Intell. Transp. Syst.* **2020**, 1–9. [CrossRef]
13. Liu, L.; Li, J.; Yue, F.; Yan, X.; Wang, F.; Bloszies, S.; Wang, Y. Effects of arbuscular mycorrhizal inoculation and biochar amendment on maize growth, cadmium uptake and soil cadmium speciation in Cd-contaminated soil. *Chemosphere* **2018**, *194*, 495–503. [CrossRef] [PubMed]
14. Yang, Y.; Liu, J.; Yao, J.; Kou, J.; Li, Z.; Wu, T.; Zhang, K.; Zhang, L.; Sun, H. Adsorption behaviors of shale oil in kerogen slit by molecular simulation. *Chem. Eng. J.* **2020**, *387*, 124054. [CrossRef]
15. Hu, X.; Chong, H.-Y.; Wang, X. Sustainability perceptions of off-site manufacturing stakeholders in Australia. *J. Clean. Prod.* **2019**, *227*, 346–354. [CrossRef]
16. Ghaemi, A.; Rezaie-Balf, M.; Adamowski, J.; Kisi, O.; Quilty, J. On the applicability of maximum overlap discrete wavelet transform integrated with MARS and M5 model tree for monthly pan evaporation prediction. *Agric. For. Meteorol.* **2019**, *278*, 107647. [CrossRef]
17. Keshtegar, B.; Heddam, S.; Sebbar, A.; Zhu, S.-P.; Trung, N.-T. SVR-RSM: A hybrid heuristic method for modeling monthly pan evaporation. *Environ. Sci. Pollut. Res.* **2019**, *26*, 35807–35826. [CrossRef] [PubMed]
18. Kisi, O.; Heddam, S. Evaporation modelling by heuristic regression approaches using only temperature data. *Hydrol. Sci. J.* **2019**, *64*, 653–672. [CrossRef]
19. Roy, D.K.; Barzegar, R.; Quilty, J.; Adamowski, J. Using ensembles of adaptive neuro-fuzzy inference system and optimization algorithms to predict reference evapotranspiration in subtropical climatic zones. *J. Hydrol.* **2020**, 125509. [CrossRef]
20. Zhang, B.; Xu, D.; Liu, Y.; Li, F.; Cai, J.; Du, L. Multi-scale evapotranspiration of summer maize and the controlling meteorological factors in north China. *Agric. For. Meteorol.* **2016**, *216*, 1–12. [CrossRef]
21. Chao, L.; Zhang, K.; Li, Z.; Zhu, Y.; Wang, J.; Yu, Z. Geographically weighted regression based methods for merging satellite and gauge precipitation. *J. Hydrol.* **2018**, *558*, 275–289. [CrossRef]

22. Chen, Y.; He, L.; Guan, Y.; Lu, H.; Li, J. Life cycle assessment of greenhouse gas emissions and water-energy optimization for shale gas supply chain planning based on multi-level approach: Case study in Barnett, Marcellus, Fayetteville, and Haynesville shales. *Energy Convers. Manag.* **2017**, *134*, 382–398. [CrossRef]
23. He, L.; Chen, Y.; Li, J. A three-level framework for balancing the tradeoffs among the energy, water, and air-emission implications within the life-cycle shale gas supply chains. *Resour. Conserv. Recycl.* **2018**, *133*, 206–228. [CrossRef]
24. Lu, H.; Tian, P.; He, L. Evaluating the global potential of aquifer thermal energy storage and determining the potential worldwide hotspots driven by socio-economic, geo-hydrologic and climatic conditions. *Renew. Sustain. Energy Rev.* **2019**, *112*, 788–796. [CrossRef]
25. Wang, Y.; Yao, M.; Ma, R.; Yuan, Q.; Yang, D.; Cui, B.; Ma, C.; Liu, M.; Hu, D. Design strategy of barium titanate/polyvinylidene fluoride-based nanocomposite films for high energy storage. *J. Mater. Chem. A* **2020**, *8*, 884–917. [CrossRef]
26. Zhang, W. Parameter Adjustment Strategy and Experimental Development of Hydraulic System for Wave Energy Power Generation. *Symmetry* **2020**, *12*, 711. [CrossRef]
27. Zhao, X.; Ye, Y.; Ma, J.; Shi, P.; Chen, H. Construction of electric vehicle driving cycle for studying electric vehicle energy consumption and equivalent emissions. *Environ. Sci. Pollut. Res.* **2020**, *27*, 37395–37409. [CrossRef]
28. Zhu, L.; Kong, L.; Zhang, C. Numerical Study on Hysteretic Behaviour of Horizontal-Connection and Energy-Dissipation Structures Developed for Prefabricated Shear Walls. *Appl. Sci.* **2020**, *10*, 1240. [CrossRef]
29. Deng, Y.; Zhang, T.; Sharma, B.K.; Nie, H. Optimization and mechanism studies on cell disruption and phosphorus recovery from microalgae with magnesium modified hydrochar in assisted hydrothermal system. *Sci. Total Environ.* **2019**, *646*, 1140–1154. [CrossRef]
30. Zhang, T.; Wu, X.; Fan, X.; Tsang, D.C.W.; Li, G.; Shen, Y. Corn waste valorization to generate activated hydrochar to recover ammonium nitrogen from compost leachate by hydrothermal assisted pretreatment. *J. Environ. Manag.* **2019**, *236*, 108–117. [CrossRef]
31. Liu, E.; Wang, X.; Zhao, W.; Su, Z.; Chen, Q. Analysis and Research on Pipeline Vibration of a Natural Gas Compressor Station and Vibration Reduction Measures. *Energy Fuels* **2020**. [CrossRef]
32. Peng, S.; Chen, Q.; Zheng, C.; Liu, E. Analysis of particle deposition in a new-type rectifying plate system during shale gas extraction. *Energy Sci. Eng.* **2020**, *8*, 702–717. [CrossRef]
33. Peng, S.; Zhang, Z.; Liu, E.; Liu, W.; Qiao, W. A new hybrid algorithm model for prediction of internal corrosion rate of multiphase pipeline. *J. Nat. Gas Sci. Eng.* **2021**, *85*, 103716. [CrossRef]
34. Liu, E.; Guo, B.; Lv, L.; Qiao, W.; Azimi, M. Numerical simulation and simplified calculation method for heat exchange performance of dry air cooler in natural gas pipeline compressor station. *Energy Sci. Eng.* **2020**, *8*, 2256–2270. [CrossRef]
35. Yang, C.; Gao, F.; Dong, M. Energy Efficiency Modeling of Integrated Energy System in Coastal Areas. *J. Coast. Res.* **2020**, *103*, 995–1001. [CrossRef]
36. Li, Z.-G.; Cheng, H.; Gu, T.-Y. Research on dynamic relationship between natural gas consumption and economic growth in China. *Struct. Chang. Econ. Dyn.* **2019**, *49*, 334–339. [CrossRef]
37. Liu, E.; Lv, L.; Yi, Y.; Xie, P. Research on the Steady Operation Optimization Model of Natural Gas Pipeline Considering the Combined Operation of Air Coolers and Compressors. *IEEE Access* **2019**, *7*, 83251–83265. [CrossRef]
38. Su, Z.; Liu, E.; Xu, Y.; Xie, P.; Shang, C.; Zhu, Q. Flow field and noise characteristics of manifold in natural gas transportation station. *Oil Gas Sci. Technol. Rev. d'IFP Energ. Nouv.* **2019**, *74*, 70. [CrossRef]
39. Chen, Y.; He, L.; Li, J.; Zhang, S. Multi-criteria design of shale-gas-water supply chains and production systems towards optimal life cycle economics and greenhouse gas emissions under uncertainty. *Comput. Chem. Eng.* **2018**, *109*, 216–235. [CrossRef]
40. Chen, Y.; Li, J.; Lu, H.; Yan, P. Coupling system dynamics analysis and risk aversion programming for optimizing the mixed noise-driven shale gas-water supply chains. *J. Clean. Prod.* **2021**, *278*, 123209. [CrossRef]
41. Cheng, X.; He, L.; Lu, H.; Chen, Y.; Ren, L. Optimal water resources management and system benefit for the Marcellus shale-gas reservoir in Pennsylvania and West Virginia. *J. Hydrol.* **2016**, *540*, 412–422. [CrossRef]
42. Zheng, S.; Lyu, Z.; Foong, L.K. Early prediction of cooling load in energy-efficient buildings through novel optimizer of shuffled complex evolution. *Eng. Comput.* **2020**, 1–15. [CrossRef]
43. Li, X.; Zhang, R.; Zhang, X.; Zhu, P.; Yao, T. Silver-Catalyzed Decarboxylative Allylation of Difluoroarylacetic Acids with Allyl Sulfones in Water. *Chem. Asian J.* **2020**, *15*, 1175–1179. [CrossRef]
44. Quan, Q.; Hao, Z.; Xifeng, H.; Jingchun, L. Research on water temperature prediction based on improved support vector regression. *Neural Comput. Appl.* **2020**, 1–10. [CrossRef]
45. Yang, M.; Sowmya, A. An Underwater Color Image Quality Evaluation Metric. *IEEE Trans. Image Process.* **2015**, *24*, 6062–6071. [CrossRef] [PubMed]
46. Cao, B.; Fan, S.; Zhao, J.; Yang, P.; Muhammad, K.; Tanveer, M. Quantum-enhanced multiobjective large-scale optimization via parallelism. *Swarm Evol. Comput.* **2020**, *57*, 100697. [CrossRef]
47. Jia, L.; Liu, B.; Zhao, Y.; Chen, W.; Mou, D.; Fu, J.; Wang, Y.; Xin, W.; Zhao, L. Structure design of MoS2@Mo2C on nitrogen-doped carbon for enhanced alkaline hydrogen evolution reaction. *J. Mater. Sci.* **2020**, *55*, 16197–16210. [CrossRef]
48. Lyu, Z.; Chai, J.; Xu, Z.; Qin, Y.; Cao, J. A Comprehensive Review on Reasons for Tailings Dam Failures Based on Case History. *Adv. Civ. Eng.* **2019**, *2019*, 4159306. [CrossRef]

49. Feng, W.; Lu, H.; Yao, T.; Yu, Q. Drought characteristics and its elevation dependence in the Qinghai–Tibet plateau during the last half-century. *Sci. Rep.* **2020**, *10*, 14323. [CrossRef]
50. Qian, J.; Feng, S.; Li, Y.; Tao, T.; Han, J.; Chen, Q.; Zuo, C. Single-shot absolute 3D shape measurement with deep-learning-based color fringe projection profilometry. *Opt. Lett.* **2020**, *45*, 1842–1845. [CrossRef] [PubMed]
51. Zenggang, X.; Zhiwen, T.; Xiaowen, C.; Xue-min, Z.; Kaibin, Z.; Conghuan, Y. Research on Image Retrieval Algorithm Based on [of Color and Shape Features. *J. Signal Process. Syst.* **2019**, 1–8. [CrossRef]
52. Zhu, Q. Research on Road Traffic Situation Awareness System Based on Image Big Data. *IEEE Intell. Syst.* **2020**, *35*, 18–26. [CrossRef]
53. Xu, S.; Wang, J.; Shou, W.; Ngo, T.; Sadick, A.-M.; Wang, X. Computer Vision Techniques in Construction: A Critical Review. *Arch. Comput. Methods Eng.* **2020**. [CrossRef]
54. Sun, Y.; Wang, J.; Wu, J.; Shi, W.; Ji, D.; Wang, X.; Zhao, X. Constraints hindering the development of high-rise modular buildings. *Appl. Sci.* **2020**, *10*, 7159. [CrossRef]
55. Chao, M.; Kai, C.; Zhiwei, Z. Research on tobacco foreign body detection device based on machine vision. *Trans. Inst. Meas. Control* **2020**, *42*, 2857–2871. [CrossRef]
56. Liu, D.; Wang, S.; Huang, D.; Deng, G.; Zeng, F.; Chen, H. Medical image classification using spatial adjacent histogram based on adaptive local binary patterns. *Comput. Biol. Med.* **2016**, *72*, 185–200. [CrossRef] [PubMed]
57. Zhang, K.; Ruben, G.B.; Li, X.; Li, Z.; Yu, Z.; Xia, J.; Dong, Z. A comprehensive assessment framework for quantifying climatic and anthropogenic contributions to streamflow changes: A case study in a typical semi-arid North China basin. *Environ. Model. Softw.* **2020**, *128*, 104704. [CrossRef]
58. Wang, B.; Zhang, B.F.; Liu, X.W.; Zou, F.C. Novel infrared image enhancement optimization algorithm combined with DFOCS. *Optik* **2020**, *224*, 165476. [CrossRef]
59. Zhao, Y.; Yan, Q.; Yang, Z.; Yu, X.; Jia, B. A Novel Artificial Bee Colony Algorithm for Structural Damage Detection. *Adv. Civ. Eng.* **2020**, *2020*, 3743089. [CrossRef]
60. Yu, H.; Shen, S.; Qian, G.; Gong, X. Packing theory and volumetrics-based aggregate gradation design method. *J. Mater. Civ. Eng.* **2020**, *32*, 04020110. [CrossRef]
61. Zhang, C.; Wang, H. Swing vibration control of suspended structures using the Active Rotary Inertia Driver system: Theoretical modeling and experimental verification. *Struct. Control Health Monit.* **2020**, *27*, e2543. [CrossRef]
62. Abedini, M.; Mutalib, A.A.; Zhang, C.; Mehrmashhadi, J.; Raman, S.N.; Alipour, R.; Momeni, T.; Mussa, M.H. Large deflection behavior effect in reinforced concrete columns exposed to extreme dynamic loads. *Front. Struct. Civ. Eng.* **2020**, *14*, 532–553. [CrossRef]
63. Mou, B.; Li, X.; Bai, Y.; Wang, L. Shear behavior of panel zones in steel beam-to-column connections with unequal depth of outer annular stiffener. *J. Struct. Eng.* **2019**, *145*, 04018247. [CrossRef]
64. Zhao, Y.; Joseph, A.J.J.M.; Zhang, Z.; Ma, C.; Gul, D.; Schellenberg, A.; Hu, N. Deterministic snap-through buckling and energy trapping in axially-loaded notched strips for compliant building blocks. *Smart Mater. Struct.* **2020**, *29*, 02LT03. [CrossRef]
65. Gholipour, G.; Zhang, C.; Mousavi, A.A. Numerical analysis of axially loaded RC columns subjected to the combination of impact and blast loads. *Eng. Struct.* **2020**, *219*, 110924. [CrossRef]
66. Qian, J.; Feng, S.; Tao, T.; Hu, Y.; Li, Y.; Chen, Q.; Zuo, C. Deep-learning-enabled geometric constraints and phase unwrapping for single-shot absolute 3D shape measurement. *APL Photonics* **2020**, *5*, 046105. [CrossRef]
67. Yang, W.; Pudasainee, D.; Gupta, R.; Li, W.; Wang, B.; Sun, L. An overview of inorganic particulate matter emission from coal/biomass/MSW combustion: Sampling and measurement, formation, distribution, inorganic composition and influencing factors. *Fuel Process. Technol.* **2020**, 106657. [CrossRef]
68. Zhang, C.-W.; Ou, J.-P.; Zhang, J.-Q. Parameter optimization and analysis of a vehicle suspension system controlled by magnetorheological fluid dampers. *Struct. Control Health Monit.* **2006**, *13*, 885–896. [CrossRef]
69. Mou, B.; Zhao, F.; Qiao, Q.; Wang, L.; Li, H.; He, B.; Hao, Z. Flexural behavior of beam to column joints with or without an overlying concrete slab. *Eng. Struct.* **2019**, *199*, 109616. [CrossRef]
70. Abedini, M.; Zhang, C. Performance Assessment of Concrete and Steel Material Models in LS-DYNA for Enhanced Numerical Simulation, A State of the Art Review. *Arch. Comput. Methods Eng.* **2020**. [CrossRef]
71. Zhang, C.; Abedini, M.; Mehrmashhadi, J. Development of pressure-impulse models and residual capacity assessment of RC columns using high fidelity Arbitrary Lagrangian-Eulerian simulation. *Eng. Struct.* **2020**, *224*, 111219. [CrossRef]
72. Yue, H.; Wang, H.; Chen, H.; Cai, K.; Jin, Y. Automatic detection of feather defects using Lie group and fuzzy Fisher criterion for shuttlecock production. *Mech. Syst. Signal Process.* **2020**, *141*, 106690. [CrossRef]
73. Zhu, G.; Wang, S.; Sun, L.; Ge, W.; Zhang, X. Output Feedback Adaptive Dynamic Surface Sliding-Mode Control for Quadrotor UAVs with Tracking Error Constraints. *Complexity* **2020**, *2020*, 8537198.
74. Xiong, Q.; Zhang, X.; Wang, W.-F.; Gu, Y. A Parallel Algorithm Framework for Feature Extraction of EEG Signals on MPI. *Comput. Math. Methods Med.* **2020**, *2020*, 9812019. [CrossRef]
75. Zhang, H.; Qu, S.; Li, H.; Luo, J.; Xu, W. A Moving Shadow Elimination Method Based on Fusion of Multi-Feature. *IEEE Access* **2020**, *8*, 63971–63982. [CrossRef]
76. Zhang, J.; Liu, B. A review on the recent developments of sequence-based protein feature extraction methods. *Curr. Bioinform.* **2019**, *14*, 190–199. [CrossRef]

77. Zhang, X.; Fan, M.; Wang, D.; Zhou, P.; Tao, D. Top-k Feature Selection Framework Using Robust 0–1 Integer Programming. *IEEE Trans. Neural Netw. Learn. Syst.* **2020**, 1–15. [CrossRef]
78. Zhao, X.; Li, D.; Yang, B.; Chen, H.; Yang, X.; Yu, C.; Liu, S. A two-stage feature selection method with its application. *Comput. Electr. Eng.* **2015**, *47*, 114–125. [CrossRef]
79. Liu, S.; Chan, F.T.S.; Ran, W. Decision making for the selection of cloud vendor: An improved approach under group decision-making with integrated weights and objective/subjective attributes. *Expert Syst. Appl.* **2016**, *55*, 37–47. [CrossRef]
80. Tian, P.; Lu, H.; Feng, W.; Guan, Y.; Xue, Y. Large decrease in streamflow and sediment load of Qinghai–Tibetan Plateau driven by future climate change: A case study in Lhasa River Basin. *CATENA* **2020**, *187*, 104340. [CrossRef]
81. Yang, L.; Chen, H. Fault diagnosis of gearbox based on RBF-PF and particle swarm optimization wavelet neural network. *Neural Comput. Appl.* **2019**, *31*, 4463–4478. [CrossRef]
82. Cao, B.; Zhao, J.; Lv, Z.; Gu, Y.; Yang, P.; Halgamuge, S.K. Multiobjective Evolution of Fuzzy Rough Neural Network via Distributed Parallelism for Stock Prediction. *IEEE Trans. Fuzzy Syst.* **2020**, *28*, 939–952. [CrossRef]
83. Shi, K.; Wang, J.; Tang, Y.; Zhong, S. Reliable asynchronous sampled-data filtering of T–S fuzzy uncertain delayed neural networks with stochastic switched topologies. *Fuzzy Sets Syst.* **2020**, *381*, 1–25. [CrossRef]
84. Shi, K.; Wang, J.; Zhong, S.; Tang, Y.; Cheng, J. Non-fragile memory filtering of T-S fuzzy delayed neural networks based on switched fuzzy sampled-data control. *Fuzzy Sets Syst.* **2020**, *394*, 40–64. [CrossRef]
85. Yang, S.; Deng, B.; Wang, J.; Li, H.; Lu, M.; Che, Y.; Wei, X.; Loparo, K.A. Scalable Digital Neuromorphic Architecture for Large-Scale Biophysically Meaningful Neural Network With Multi-Compartment Neurons. *IEEE Trans. Neural Netw. Learn. Syst.* **2020**, *31*, 148–162. [CrossRef]
86. Adeli, H. Neural networks in civil engineering: 1989–2000. *Comput. Aided Civ. Infrastruct. Eng.* **2001**, *16*, 126–142. [CrossRef]
87. Hornik, K.; Stinchcombe, M.; White, H. Multilayer feedforward networks are universal approximators. *Neural Netw.* **1989**, *2*, 359–366. [CrossRef]
88. Lv, Z.; Qiao, L. Deep belief network and linear perceptron based cognitive computing for collaborative robots. *Appl. Soft Comput.* **2020**, *92*, 106300. [CrossRef]
89. Xu, M.; Li, T.; Wang, Z.; Deng, X.; Yang, R.; Guan, Z. Reducing Complexity of HEVC: A Deep Learning Approach. *IEEE Trans. Image Process.* **2018**, *27*, 5044–5059. [CrossRef]
90. Li, T.; Xu, M.; Zhu, C.; Yang, R.; Wang, Z.; Guan, Z. A Deep Learning Approach for Multi-Frame In-Loop Filter of HEVC. *IEEE Trans. Image Process.* **2019**, *28*, 5663–5678. [CrossRef]
91. Qiu, T.; Shi, X.; Wang, J.; Li, Y.; Qu, S.; Cheng, Q.; Cui, T.; Sui, S. Deep Learning: A Rapid and Efficient Route to Automatic Metasurface Design. *Adv. Sci.* **2019**, *6*, 1900128. [CrossRef]
92. Chen, H.; Chen, A.; Xu, L.; Xie, H.; Qiao, H.; Lin, Q.; Cai, K. A deep learning CNN architecture applied in smart near-infrared analysis of water pollution for agricultural irrigation resources. *Agric. Water Manag.* **2020**, *240*, 106303. [CrossRef]
93. Zhang, X.; Jiang, R.; Wang, T.; Wang, J. Recursive Neural Network for Video Deblurring. *IEEE Trans. Circuits Syst. Video Technol.* **2020**. [CrossRef]
94. de Rosa, G.H.; Papa, J.P.; Yang, X.-S. Handling dropout probability estimation in convolution neural networks using meta-heuristics. *Soft Comput.* **2018**, *22*, 6147–6156. [CrossRef]
95. Xia, J.; Chen, H.; Li, Q.; Zhou, M.; Chen, L.; Cai, Z.; Fang, Y.; Zhou, H. Ultrasound-based differentiation of malignant and benign thyroid Nodules: An extreme learning machine approach. *Comput. Methods Programs Biomed.* **2017**, *147*, 37–49. [CrossRef] [PubMed]
96. Hu, L.; Hong, G.; Ma, J.; Wang, X.; Chen, H. An efficient machine learning approach for diagnosis of paraquat-poisoned patients. *Comput. Biol. Med.* **2015**, *59*, 116–124. [CrossRef] [PubMed]
97. Wang, S.-J.; Chen, H.-L.; Yan, W.-J.; Chen, Y.-H.; Fu, X. Face recognition and micro-expression recognition based on discriminant tensor subspace analysis plus extreme learning machine. *Neural Process. Lett.* **2014**, *39*, 25–43. [CrossRef]
98. Chen, H.-L.; Wang, G.; Ma, C.; Cai, Z.-N.; Liu, W.-B.; Wang, S.-J. An efficient hybrid kernel extreme learning machine approach for early diagnosis of Parkinson's disease. *Neurocomputing* **2016**, *184*, 131–144. [CrossRef]
99. Wojtkiewicz, J.; Katragadda, S.; Gottumukkala, R. A Concept-Drift Based Predictive-Analytics Framework: Application for Real-Time Solar Irradiance Forecasting. In Proceedings of the 2018 IEEE International Conference on Big Data (Big Data), Seattle, WA, USA, 10–13 December 2018; pp. 5462–5464.
100. Lee, J.; Wang, W.; Harrou, F.; Sun, Y. Reliable solar irradiance prediction using ensemble learning-based models: A comparative study. *Energy Convers. Manag.* **2020**, *208*, 112582. [CrossRef]
101. Wang, H.; Sun, J.; Wang, W. Photovoltaic Power Forecasting Based on EEMD and a Variable-Weight Combination Forecasting Model. *Sustainability* **2018**, *10*, 2627. [CrossRef]
102. Massimo, A.; Dell'Isola, M.; Frattolillo, A.; Ficco, G. Development of a geographical information system (GIS) for the integration of solar energy in the energy planning of a wide area. *Sustainability* **2014**, *6*, 5730–5744. [CrossRef]
103. Salcedo-Sanz, S.; Cornejo-Bueno, L.; Prieto, L.; Paredes, D.; García-Herrera, R. Feature selection in machine learning prediction systems for renewable energy applications. *Renew. Sustain. Energy Rev.* **2018**, *90*, 728–741. [CrossRef]
104. Barrera, J.M.; Reina, A.; Maté, A.; Trujillo, J.C. Solar Energy Prediction Model Based on Artificial Neural Networks and Open Data. *Sustainability* **2020**, *12*, 6915. [CrossRef]

105. Yaïci, W.; Longo, M.; Entchev, E.; Foiadelli, F. Simulation study on the effect of reduced inputs of artificial neural networks on the predictive performance of the solar energy system. *Sustainability* **2017**, *9*, 1382. [CrossRef]
106. Yadav, A.K.; Malik, H.; Chandel, S. Application of rapid miner in ANN based prediction of solar radiation for assessment of solar energy resource potential of 76 sites in Northwestern India. *Renew. Sustain. Energy Rev.* **2015**, *52*, 1093–1106. [CrossRef]
107. Meenal, R.; Selvakumar, A.I. Assessment of SVM, empirical and ANN based solar radiation prediction models with most influencing input parameters. *Renew. Energy* **2018**, *121*, 324–343. [CrossRef]
108. Mohammadi, K.; Shamshirband, S.; Kamsin, A.; Lai, P.; Mansor, Z. Identifying the most significant input parameters for predicting global solar radiation using an ANFIS selection procedure. *Renew. Sustain. Energy Rev.* **2016**, *63*, 423–434. [CrossRef]
109. Quej, V.H.; Almorox, J.; Arnaldo, J.A.; Saito, L. ANFIS, SVM and ANN soft-computing techniques to estimate daily global solar radiation in a warm sub-humid environment. *J. Atmos. Sol. Terr. Phys.* **2017**, *155*, 62–70. [CrossRef]
110. Houssein, E.H. Machine Learning and Meta-heuristic Algorithms for Renewable Energy: A Systematic Review. In *Advanced Control and Optimization Paradigms for Wind Energy Systems*; Springer: Berlin/Heidelberg, Germany, 2019; pp. 165–187.
111. Corizzo, R.; Ceci, M.; Fanaee, T.H.; Gama, J. Multi-aspect renewable energy forecasting. *Inf. Sci.* **2021**, *546*, 701–722. [CrossRef]
112. Liu, H.; Chen, C.; Lv, X.; Wu, X.; Liu, M. Deterministic wind energy forecasting: A review of intelligent predictors and auxiliary methods. *Energy Convers. Manag.* **2019**, *195*, 328–345. [CrossRef]
113. Cavalcante, L.; Bessa, R.J.; Reis, M.; Browell, J. LASSO vector autoregression structures for very short-term wind power forecasting. *Wind Energy* **2017**, *20*, 657–675. [CrossRef]
114. Bessa, R.J.; Trindade, A.; Silva, C.S.P.; Miranda, V. Probabilistic solar power forecasting in smart grids using distributed information. *Int. J. Electr. Power Energy Syst.* **2015**, *72*, 16–23. [CrossRef]
115. Elsheikh, A.H.; Sharshir, S.W.; Abd Elaziz, M.; Kabeel, A.; Guilan, W.; Haiou, Z. Modeling of solar energy systems using artificial neural network: A comprehensive review. *Solar Energy* **2019**, *180*, 622–639. [CrossRef]
116. Akhter, M.N.; Mekhilef, S.; Mokhlis, H.; Shah, N.M. Review on forecasting of photovoltaic power generation based on machine learning and metaheuristic techniques. *IET Renew. Power Gener.* **2019**, *13*, 1009–1023. [CrossRef]
117. Moayedi, H.; Mehrabi, M.; Mosallanezhad, M.; Rashid, A.S.A.; Pradhan, B. Modification of landslide susceptibility mapping using optimized PSO-ANN technique. *Eng. Comput.* **2019**, *35*, 967–984. [CrossRef]
118. Tu, J.; Chen, H.; Liu, J.; Heidari, A.A.; Zhang, X.; Wang, M.; Ruby, R.; Pham, Q.-V. Evolutionary biogeography-based whale optimization methods with communication structure: Towards measuring the balance. *Knowl. Based Syst.* **2021**, *212*, 106642. [CrossRef]
119. Wang, M.; Chen, H.J.A.S.C. Chaotic multi-swarm whale optimizer boosted support vector machine for medical diagnosis. *Appl. Soft Comput.* **2020**, *88*, 105946. [CrossRef]
120. Zhao, X.; Zhang, X.; Cai, Z.; Tian, X.; Wang, X.; Huang, Y.; Chen, H.; Hu, L. Chaos enhanced grey wolf optimization wrapped ELM for diagnosis of paraquat-poisoned patients. *Comput. Biol. Chem.* **2019**, *78*, 481–490. [CrossRef]
121. Hu, J.; Chen, H.; Heidari, A.A.; Wang, M.; Zhang, X.; Chen, Y.; Pan, Z.J.K.-B.S. Orthogonal learning covariance matrix for defects of grey wolf optimizer: Insights, balance, diversity, and feature selection. *Knowl. Based Syst.* **2020**, *213*, 106684. [CrossRef]
122. Cao, B.; Zhao, J.; Gu, Y.; Ling, Y.; Ma, X. Applying graph-based differential grouping for multiobjective large-scale optimization. *Swarm Evol. Comput.* **2020**, *53*, 100626. [CrossRef]
123. Cao, B.; Dong, W.; Lv, Z.; Gu, Y.; Singh, S.; Kumar, P. Hybrid Microgrid Many-Objective Sizing Optimization With Fuzzy Decision. *IEEE Trans. Fuzzy Syst.* **2020**, *28*, 2702–2710. [CrossRef]
124. Cao, B.; Wang, X.; Zhang, W.; Song, H.; Lv, Z. A Many-Objective Optimization Model of Industrial Internet of Things Based on Private Blockchain. *IEEE Netw.* **2020**, *34*, 78–83. [CrossRef]
125. Cao, B.; Zhao, J.; Gu, Y.; Fan, S.; Yang, P. Security-Aware Industrial Wireless Sensor Network Deployment Optimization. *IEEE Trans. Ind. Inform.* **2020**, *16*, 5309–5316. [CrossRef]
126. Shan, W.; Qiao, Z.; Heidari, A.A.; Chen, H.; Turabieh, H.; Teng, Y.J.K.-B.S. Double adaptive weights for stabilization of moth flame optimizer: Balance analysis, engineering cases, and medical diagnosis. *Knowl. Based Syst.* **2020**, *214*, 106728. [CrossRef]
127. Xu, Y.; Chen, H.; Luo, J.; Zhang, Q.; Jiao, S.; Zhang, X.J.I.S. Enhanced Moth-flame optimizer with mutation strategy for global optimization. *Inf. Sci.* **2019**, *492*, 181–203. [CrossRef]
128. Wang, M.; Chen, H.; Yang, B.; Zhao, X.; Hu, L.; Cai, Z.; Huang, H.; Tong, C.J.N. Toward an optimal kernel extreme learning machine using a chaotic moth-flame optimization strategy with applications in medical diagnoses. *Neurocomputing* **2017**, *267*, 69–84. [CrossRef]
129. Bacanin, N.; Bezdan, T.; Tuba, E.; Strumberger, I.; Tuba, M. Monarch Butterfly Optimization Based Convolutional Neural Network Design. *Mathematics* **2020**, *8*, 936. [CrossRef]
130. Zhang, Y.; Liu, R.; Wang, X.; Chen, H.; Li, C.J. Boosted binary Harris hawks optimizer and feature selection. *Eng. Comput.* **2020**, *25*, 26. [CrossRef]
131. Chen, H.; Heidari, A.A.; Chen, H.; Wang, M.; Pan, Z.; Gandomi, A.H. Multi-population differential evolution-assisted Harris hawks optimization: Framework and case studies. *Future Gener. Comput. Syst.* **2020**, *111*, 175–198. [CrossRef]
132. Xu, X.; Chen, H.-L. Adaptive computational chemotaxis based on field in bacterial foraging optimization. *Soft Comput.* **2014**, *18*, 797–807. [CrossRef]
133. Sun, G.; Yang, B.; Yang, Z.; Xu, G. An adaptive differential evolution with combined strategy for global numerical optimization. *Soft Comput.* **2019**, *24*, 6277–6296. [CrossRef]

134. Yu, C.; Chen, M.; Cheng, K.; Zhao, X.; Ma, C.; Kuang, F.; Chen, H. SGOA: Annealing-behaved grasshopper optimizer for global tasks. *Eng. Comput.* **2021**, 1–28. [CrossRef]
135. Shen, L.; Chen, H.; Yu, Z.; Kang, W.; Zhang, B.; Li, H.; Yang, B.; Liu, D.J.K. Evolving support vector machines using fruit fly optimization for medical data classification. *Knowl. Based Syst.* **2016**, *96*, 61–75. [CrossRef]
136. Qu, S.; Han, Y.; Wu, Z.; Raza, H. Consensus Modeling with Asymmetric Cost Based on Data-Driven Robust Optimization. *Group Decis. Negot.* **2020**. [CrossRef]
137. Fu, X.; Pace, P.; Aloi, G.; Yang, L.; Fortino, G. Topology Optimization Against Cascading Failures on Wireless Sensor Networks Using a Memetic Algorithm. *Comput. Netw.* **2020**, *177*, 107327. [CrossRef]
138. Cao, B.; Zhao, J.; Yang, P.; Gu, Y.; Muhammad, K.; Rodrigues, J.J.P.C.; Albuquerque, V.H.C. Multiobjective 3-D Topology Optimization of Next-Generation Wireless Data Center Network. *IEEE Trans. Ind. Inform.* **2020**, *16*, 3597–3605. [CrossRef]
139. Chen, H.; Qiao, H.; Xu, L.; Feng, Q.; Cai, K. A Fuzzy Optimization Strategy for the Implementation of RBF LSSVR Model in Vis–NIR Analysis of Pomelo Maturity. *IEEE Trans. Ind. Inform.* **2019**, *15*, 5971–5979. [CrossRef]
140. Abedinia, O.; Amjady, N.; Ghadimi, N. Solar energy forecasting based on hybrid neural network and improved metaheuristic algorithm. *Comput. Intell.* **2018**, *34*, 241–260. [CrossRef]
141. Galván, I.M.; Valls, J.M.; Cervantes, A.; Aler, R. Multi-objective evolutionary optimization of prediction intervals for solar energy forecasting with neural networks. *Inf. Sci.* **2017**, *418*, 363–382. [CrossRef]
142. Zhao, Y.; Moayedi, H.; Bahiraei, M.; Foong, L.K. Employing TLBO and SCE for optimal prediction of the compressive strength of concrete. *Smart Struct. Syst.* **2020**, *26*, 753.
143. Halabi, L.M.; Mekhilef, S.; Hossain, M. Performance evaluation of hybrid adaptive neuro-fuzzy inference system models for predicting monthly global solar radiation. *Appl. Energy* **2018**, *213*, 247–261. [CrossRef]
144. Vaisakh, T.; Jayabarathi, R. Analysis on intelligent machine learning enabled with meta-heuristic algorithms for solar irradiance prediction. *Evol. Intell.* **2020**, 1–20. [CrossRef]
145. Louzazni, M.; Khouya, A.; Amechnoue, K.; Gandelli, A.; Mussetta, M.; Crăciunescu, A. Metaheuristic algorithm for photovoltaic parameters: Comparative study and prediction with a firefly algorithm. *Appl. Sci.* **2018**, *8*, 339. [CrossRef]
146. Bechouat, M.; Younsi, A.; Sedraoui, M.; Soufi, Y.; Yousfi, L.; Tabet, I.; Touafek, K. Parameters identification of a photovoltaic module in a thermal system using meta-heuristic optimization methods. *Int. J. Energy Environ. Eng.* **2017**, *8*, 331–341. [CrossRef]
147. Abdalla, O.; Rezk, H.; Ahmed, E.M. Wind driven optimization algorithm based global MPPT for PV system under non-uniform solar irradiance. *Sol. Energy* **2019**, *180*, 429–444. [CrossRef]
148. Elsheikh, A.; Abd Elaziz, M. Review on applications of particle swarm optimization in solar energy systems. *Int. J. Environ. Sci. Technol.* **2019**, *16*, 1159–1170. [CrossRef]
149. Aybar-Ruiz, A.; Jiménez-Fernández, S.; Cornejo-Bueno, L.; Casanova-Mateo, C.; Sanz-Justo, J.; Salvador-González, P.; Salcedo-Sanz, S. A novel grouping genetic algorithm–extreme learning machine approach for global solar radiation prediction from numerical weather models inputs. *Sol. Energy* **2016**, *132*, 129–142. [CrossRef]
150. Khosravi, A.; Syri, S. Modeling of geothermal power system equipped with absorption refrigeration and solar energy using multilayer perceptron neural network optimized with imperialist competitive algorithm. *J. Clean. Prod.* **2020**, *276*, 124216. [CrossRef]
151. Song, Y.; Lu, J.; Lu, H.; Zhang, G. Fuzzy clustering-based adaptive regression for drifting data streams. *IEEE Trans. Fuzzy Syst.* **2019**, *28*, 544–557. [CrossRef]
152. Kamble, M.; Ghosh, S.; Patel, P. Solar Irradiance Prediction using Meteorological Data by Ensemble Models. In Proceedings of the 2nd International Conference on Data, Engineering and Applications (IDEA), Bhopal, India, 28–29 February 2020; pp. 1–6.
153. Abedinpourshotorban, H.; Shamsuddin, S.M.; Beheshti, Z.; Jawawi, D.N. Electromagnetic field optimization: A physics-inspired metaheuristic optimization algorithm. *Swarm Evol. Comput.* **2016**, *26*, 8–22. [CrossRef]
154. Bouchekara, H.; Zellagui, M.; Abido, M.A. Optimal coordination of directional overcurrent relays using a modified electromagnetic field optimization algorithm. *Appl. Soft Comput.* **2017**, *54*, 267–283. [CrossRef]
155. Bouchekara, H. Solution of the optimal power flow problem considering security constraints using an improved chaotic electromagnetic field optimization algorithm. *Neural Comput. Appl.* **2020**, *32*, 2683–2703. [CrossRef]
156. Duan, Q.; Gupta, V.K.; Sorooshian, S. Shuffled complex evolution approach for effective and efficient global minimization. *J. Optim. Theory Appl.* **1993**, *76*, 501–521. [CrossRef]
157. Eusuff, M.M.; Lansey, K.E. Optimization of water distribution network design using the shuffled frog leaping algorithm. *J. Water Resour. Plan. Manag.* **2003**, *129*, 210–225. [CrossRef]
158. Ma, X.; Foong, L.K.; Morasaei, A.; Ghabussi, A.; Lyu, Z. Swarm-based hybridizations of neural network for predicting the concrete strength. *Smart Struct. Syst.* **2020**, *26*, 241–251.
159. Gao, X.; Cui, Y.; Hu, J.; Xu, G.; Wang, Z.; Qu, J.; Wang, H. Parameter extraction of solar cell models using improved shuffled complex evolution algorithm. *Energy Convers. Manag.* **2018**, *157*, 460–479. [CrossRef]
160. Moayedi, H.; Bui, D.T.; Thi Ngo, P.T. Shuffled frog leaping algorithm and wind-driven optimization technique modified with multilayer perceptron. *Appl. Sci.* **2020**, *10*, 689. [CrossRef]
161. Majeed, K.; Qyyum, M.A.; Nawaz, A.; Ahmad, A.; Naqvi, M.; He, T.; Lee, M. Shuffled Complex Evolution-Based Performance Enhancement and Analysis of Cascade Liquefaction Process for Large-Scale LNG Production. *Energies* **2020**, *13*, 2511. [CrossRef]

162. Bayat, P.; Afrakhte, H. A purpose-oriented shuffled complex evolution optimization algorithm for energy management of multi-microgrid systems considering outage duration uncertainty. *J. Intell. Fuzzy Syst.* **2020**, *38*, 1–18. [CrossRef]
163. Siahbalaee, J.; Rezanejad, N.; Gharehpetian, G.B. Reconfiguration and DG Sizing and Placement Using Improved Shuffled Frog Leaping Algorithm. *Electr. Power Compon. Syst.* **2020**, 1–14. [CrossRef]
164. Gandhi, B.R.; Bhattacharjya, R. Introduction to Shuffled Frog Leaping Algorithm and Its Sensitivity to the Parameters of the Algorithm. In *Nature-Inspired Methods for Metaheuristics Optimization*; Springer: Berlin/Heidelberg, Germany, 2020; pp. 105–117.